



Article

Temporal Evolution of Defects and Related Electric Properties in He-Irradiated $\text{YBa}_2\text{Cu}_3\text{O}_{7-\delta}$ Thin Films

Sandra Keppert ¹, Bernd Aichner ², Philip Rohringer ^{2,†}, Marius-Aurel Bodea ^{1,‡}, Benedikt Müller ³, Max Karrer ³, Reinhold Kleiner ³, Edward Goldobin ³, Dieter Koelle ³, Johannes D. Pedarnig ¹ and Wolfgang Lang ^{2,*}

- ¹ Institute of Applied Physics, Johannes Kepler University Linz, 4040 Linz, Austria; sandra.keppert@jku.at (S.K.); johannes.pedarnig@jku.at (J.D.P.)
² Faculty of Physics, University of Vienna, 1090 Vienna, Austria; bernd.aichner@univie.ac.at (B.A.)
³ Physikalisches Institut, Center for Quantum Science (CQ) and LISA⁺, University of Tübingen, 72076 Tübingen, Germany; kleiner@uni-tuebingen.de (R.K.); gold@uni-tuebingen.de (E.G.); koelle@uni-tuebingen.de (D.K.)
* Correspondence: wolfgang.lang@univie.ac.at
† Current address: Austrian Patent Office, 1200 Vienna, Austria.
‡ Current address: Infineon Technologies Austria AG, 9500 Villach, Austria.

Abstract: Thin films of the superconductor $\text{YBa}_2\text{Cu}_3\text{O}_{7-\delta}$ (YBCO) were modified by low-energy light-ion irradiation employing collimated or focused He^+ beams, and the long-term stability of irradiation-induced defects was investigated. For films irradiated with collimated beams, the resistance was measured in situ during and after irradiation and analyzed using a phenomenological model. The formation and stability of irradiation-induced defects are highly influenced by temperature. Thermal annealing experiments conducted in an Ar atmosphere at various temperatures demonstrated a decrease in resistivity and allowed us to determine diffusion coefficients and the activation energy $\Delta E = (0.31 \pm 0.03)$ eV for diffusive oxygen rearrangement within the YBCO unit cell basal plane. Additionally, thin YBCO films, nanostructured by focused He^+ -beam irradiation into vortex pinning arrays, displayed significant commensurability effects in magnetic fields. Despite the strong modulation of defect densities in these pinning arrays, oxygen diffusion during room-temperature annealing over almost six years did not compromise the signatures of vortex matching, which remained precisely at their magnetic fields predicted by the pattern geometry. Moreover, the critical current increased substantially within the entire magnetic field range after long-term storage in dry air. These findings underscore the potential of ion irradiation in tailoring the superconducting properties of thin YBCO films.

Keywords: cuprate superconductor; helium-ion irradiation; long-term stability; irradiation damage healing; vortex pinning; room-temperature annealing; diffusion coefficients; activation energy; commensurability effects

1. Introduction

High-temperature superconductors (HTSCs) are fascinating and are studied intensively due to their unconventional superconductivity. Among the HTSCs, $\text{YBa}_2\text{Cu}_3\text{O}_{7-\delta}$ (YBCO) is a popular choice due to its easy-to-fabricate and non-toxic nature, as well as its high critical temperature above the boiling point of liquid nitrogen. Various experiments have been conducted using masked or focused ion irradiation to modify the superconducting properties of YBCO and observe novel phenomena. These experiments include the creation of Josephson junctions [1–5], nanoscale superconducting quantum interference devices [6,7], superconducting quantum interference filters [8], and the manipulation of Abrikosov vortex behavior through the fabrication of artificial periodic columnar defects,

arXiv:2407.14189v1 [cond-mat.supr-con] 19 Jul 2024



Citation: Keppert, S.; Aichner, B.; Rohringer, P.; Bodea, M.-A.; Müller, B.; Karrer, M.; Kleiner, R.; Goldobin, E.; Koelle, D.; Pedarnig, J.D.; et al. Temporal Evolution of Defects and Related Electric Properties in He-Irradiated $\text{YBa}_2\text{Cu}_3\text{O}_{7-\delta}$ Thin Films. *Int. J. Mol. Sci.* **2024**, *25*, 7877. <https://doi.org/10.3390/ijms25147877>

Academic Editor: Michal Cichomski

Received: 3 July 2024

Revised: 15 July 2024

Accepted: 16 July 2024

Published: 18 July 2024



Copyright: © 2024 by the authors. Licensee MDPI, Basel, Switzerland. This article is an open access article distributed under the terms and conditions of the Creative Commons Attribution (CC BY) license (<https://creativecommons.org/licenses/by/4.0/>).

which serve as pinning centers for vortices [9–14] due to a local suppression of superconductivity [15].

Ion-beam structuring of YBCO using light elements such as He^+ ions has advantages over wet-chemical lithography and conventional ion-beam milling using Ga. Heavy ions with moderate energy are unsuitable as they have a limited penetration depth and can implant even into thin films, while swift heavy ions produce randomly distributed amorphous channels in YBCO [16]. Irradiation with electrons [17] and protons [18] would require an impractically high dose per defect column to achieve a significant pinning effect. In contrast, He^+ ions with energies of at least 30 keV can penetrate through thin YBCO films and create columns of point defects with reasonable doses. Furthermore, the minimal lateral straggle of their trajectory makes them an ideal choice [14,19].

Thorough investigations on the long-term stability of ion irradiation-induced modification of YBCO are essential for potential technical applications of the modified material. However, there is a scarcity of data on the temporal evolution of electrical properties immediately following ion irradiation and after long-term storage at ambient conditions. Research has been conducted on the time-dependent properties of Josephson junctions created by focused He^+ -ion-beam (He-FIB) irradiation [20], along with the effects of post-annealing in an oxygen atmosphere [20,21]. Additionally, the interplay between defect healing and exposure to visible light in He^+ -ion-irradiated YBCO films has been investigated [22].

In this study, we investigate the relaxation of irradiation-induced changes in the superconducting properties. Firstly, we report on the results of in situ resistance measurements during and after the irradiation process using a collimated ion beam. We also discuss the impact of sample temperature on defect formation and relaxation. Next, we investigate the thermal annealing of the irradiated YBCO films in an inert gas atmosphere and study the relaxation of defects through oxygen diffusion within the material. Finally, we report on the long-term stability of dense pinning arrays in YBCO films that were fabricated by He-FIB irradiation using a helium ion microscope (HIM). These nanostructured YBCO films show vortex matching in applied magnetic fields [13,14], and we demonstrate the long-term stability of these matching effects together with an overall increase in the critical current.

2. Results and Discussion

2.1. Defect Formation and Relaxation during and after He^+ Irradiation

In this section, we report on the modification of 240 nm thick YBCO films irradiated at different sample temperatures using a collimated He^+ beam. The formation of irradiation-induced defects in the YBCO films was monitored in situ by measuring the film's electrical resistance during and after the 75 keV He^+ irradiation. The critical temperature before irradiation was $T_{c0} = 85$ K, where T_{c0} is the temperature at which the resistance drops below the experimental resolution. YBCO bridge 1 was irradiated at a sample temperature of $T = 295$ K with an ion-beam current density of $J_B = 0.102 \mu\text{A}/\text{cm}^2$ for an irradiation time of $t_{ir1} = 26.27$ min (red line in Figure 1). An ion fluence $\Phi = 1.0 \cdot 10^{15}$ ions/ cm^2 was applied.

The resistance of bridge 1, $R_1(t)$, significantly increased during He^+ irradiation, reaching a final value of the normalized resistance $R_1(t_{ir1})/R_1(0) = 4.01$ at time $t = t_{ir1}$ when the irradiation ended. The resistance increase during irradiation showed a slightly superlinear behavior over time. We attribute this increase in resistance to the displacement of atoms, mainly oxygen atoms in CuO chains [23], distorting the YBCO unit cells, while the overall oxygen content in the films remains unchanged. It is known that such an increase in resistance can occur exclusively due to the disorder of oxygen atoms without any oxygen loss [24]. After the irradiation, the bridge resistance slightly relaxed from its maximum value, and it was reduced by approximately 7.8% at time $t = 110$ min.

In a contrasting experiment, YBCO film bridge 2 was irradiated with He^+ ions at a low temperature of $T = 100$ K using a cryogenic sample holder. The sample was kept at 100 K throughout the entire measurement. The ion current density was slightly

higher at $J_B = 0.134 \mu\text{A}/\text{cm}^2$ (red line in Figure 2). Therefore, a shorter irradiation time $t_{ir2} = 20.02 \text{ min}$ was used in order to reach the same fluence of $\Phi = 1.0 \cdot 10^{15} \text{ ions}/\text{cm}^2$.

The impact of low-temperature He^+ irradiation is much stronger than at room temperature. The resistance $R_2(t)$ shows a huge and highly superlinear increase in YBCO film bridge 2. The normalized resistance was $R_2(t_{ir2})/R_2(0) = 81.2$ at time $t = t_{ir2}$ when irradiation was stopped. In strong contrast to the room-temperature experiment, no reduction in the bridge resistance was observed later on ($t > t_{ir2}$) when the sample was kept at a low temperature. A related work using He^+ -ion energies of 500 keV supports our results, as no relaxation of resistance was found for temperatures below 250 K [25].

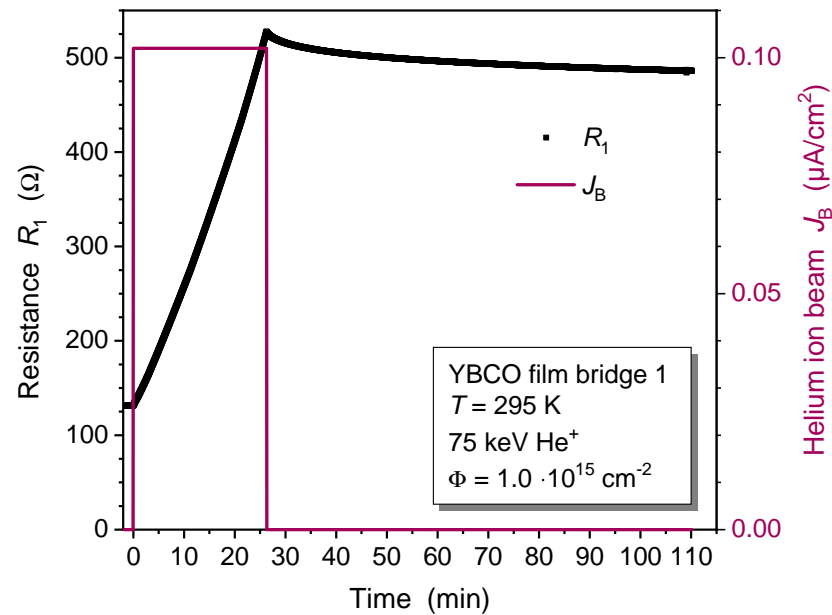


Figure 1. In-situ resistance measurement of YBCO thin film bridge 1 during and after 75 keV He^+ -ion irradiation at a temperature of $T = 295 \text{ K}$. A collimated He^+ -ion beam with a current density $J_B = 0.102 \mu\text{A}/\text{cm}^2$ (red line) and a fluence $\Phi = 1.0 \cdot 10^{15} \text{ ions}/\text{cm}^2$ was used for the irradiation.

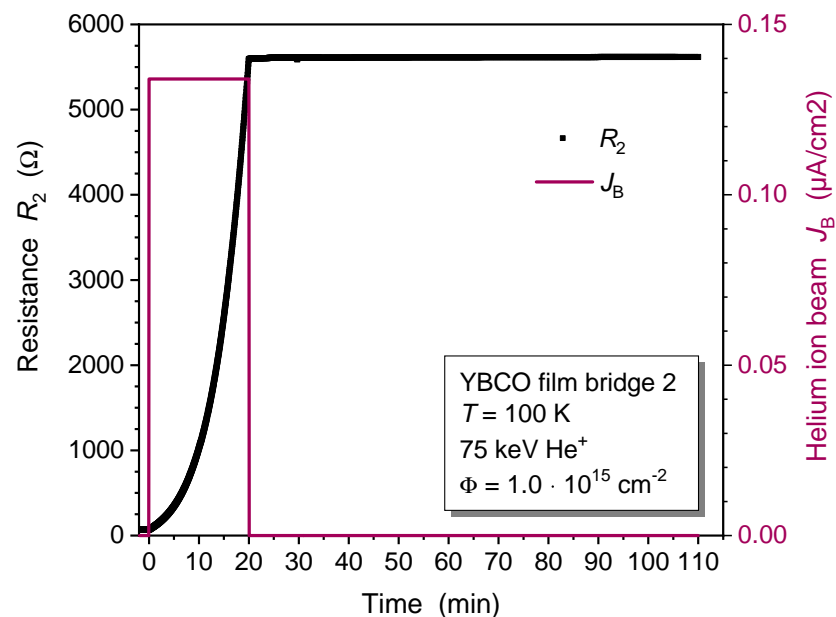


Figure 2. In-situ resistance measurement of YBCO thin film bridge 2 during and after 75 keV He^+ -ion irradiation at a temperature of $T = 100 \text{ K}$. A collimated He^+ -ion beam with a current density $J_B = 0.134 \mu\text{A}/\text{cm}^2$ (red line) and a fluence $\Phi = 1.0 \cdot 10^{15} \text{ ions}/\text{cm}^2$ was used for the irradiation.

After being exposed to ion irradiation and stored at $T = 100$ K, bridge 2 was slowly warmed up to room temperature. The changes in resistance R_2 and temperature T over time are shown in Figure 3. Remarkably, the resistance decreased from $R_2(100\text{ K}) = 5590\ \Omega$ after irradiation to $R_2(295\text{ K}) = 926\ \Omega$ as the sample warmed up. The correlation of resistance R_2 with temperature T in the inset of Figure 3 clearly indicates a thermally activated relaxation of irradiation-induced defects in the YBCO film. For comparison, the resistance of non-irradiated YBCO would have *increased* by approximately a factor of three within the same temperature interval. However, the fact that R_2 did not relax to the initial value before irradiation suggests that not all defects were healed.

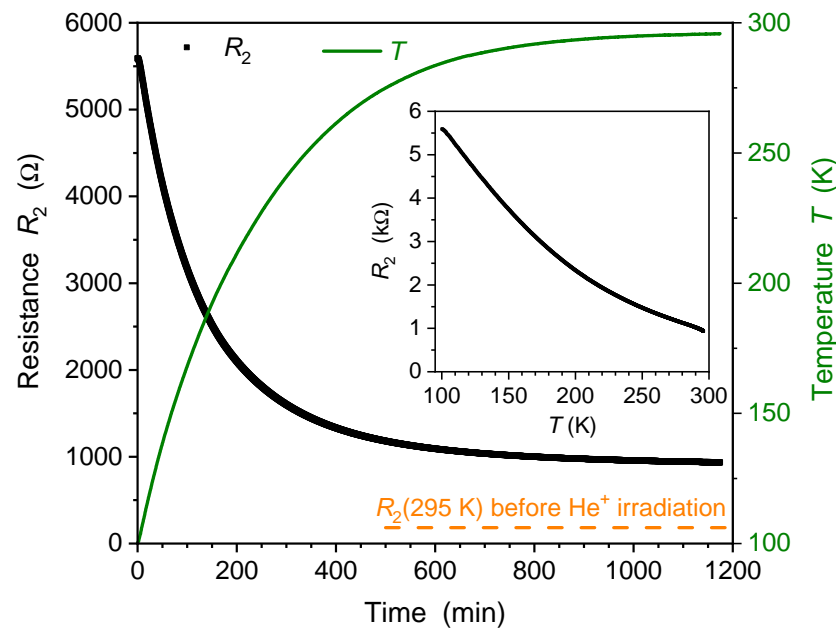


Figure 3. Resistance R_2 and temperature T of the ion-irradiated YBCO bridge 2 during warming up from 100 K to 295 K. The room-temperature resistance before ion irradiation $R_2(295\text{K})$ is indicated by an orange dotted line. Inset: R_2 as a function of temperature.

After the warm-up, the resistance $R_2(295\text{K}) = 926\ \Omega$ was significantly higher than the bridge resistance before irradiation, $R_2(295\text{K}) = 182\ \Omega$, as indicated by the dotted line in Figure 3. Even after a storage period of 14,000 min (almost 10 days) at room temperature, the resistance remained elevated at $R_2(295\text{K}) = 836\ \Omega$. The ratio of R_2 values measured before irradiation and after extended storage was 4.6. For comparison, the equivalent ratio for YBCO bridge 1, subjected to irradiation and subsequent relaxation at room temperature, was 3.7, a value similar to that of bridge 2. These results lead to the conclusion that 75 keV He^+ irradiation of YBCO thin films leads to defects with long-term stability at room temperature. Furthermore, it supports the assertion that beyond a certain defect density, room temperature is not high enough to provide the necessary energy for the complete healing of defects following irradiation [26,27].

The dependence of thin film resistance on ion fluence has been modeled only very rarely in the literature. For NiAl metal alloy films that were irradiated at $T = 77$ K with 540 keV Bi, 360 keV Xe, 120 keV Ar, and 180 keV He ions, the observed change in film resistivity was described by a model [28–30]. The fraction of ion-modified material in the film was assumed to follow the Johnson–Mehl–Avrami–Kolmogorov (JMAK) equation, which describes the temporal evolution of phase transformation of solids under isothermal conditions [31]. The change in film resistivity was assumed to be proportional to this damaged fraction [28]. However, the ion-induced change of NiAl resistivity was small and qualitatively very different from our results on YBCO films (Figures 1 and 2), and that model was therefore not applicable to fit our data.

To model the increase in YBCO thin film resistance during ion irradiation, we propose another phenomenological model that takes into account the spatial distribution of irradiation-induced defects and the volume fraction of defective material in the film. When low-energy light ions impinge on the sample, they create point-like defects in the YBCO thin film. We assume that YBCO unit cells containing an irradiation defect have increased electrical resistivity $\rho + \Delta\rho$ compared to the resistivity ρ of pristine unit cells. To simplify the model, we consider that multiple defects in the same unit cell have the same impact as a single defect. The fraction f of material with irradiation defects depends on the time t the sample is exposed to the ion beam, where $0 \leq f(t) \leq 1$. The resistance of the irradiated film $R(t)$, normalized to the resistance of the pristine film R_0 , is then given by

$$\frac{R(t)}{R_0} = 1 + \frac{f(t)r}{1 + r(1 - f(t))^d}. \quad (1)$$

The normalized resistance depends on the increase in resistivity $r = \Delta\rho/\rho$, the spatial distribution of defects described by parameter d , and the fraction f . The fraction of ion-modified material is expressed as $f(t) = 1 - \exp(-t/\tau)$, where τ is a time constant. This ansatz corresponds to the JMAK model in its simplest form, and it takes into account that the fraction of sample material to be modified by irradiation is finite ($f \leq 1$). The dimensionality parameter d characterizes, for instance, a two-dimensional (2D) random distribution of columnar defects extending through the entire depth of the film ($d = 1/2$) or a three-dimensional (3D) random distribution of point-like defects in the film ($d = 2/3$). A series and a parallel connection of two resistors would be described by $d = 0$ and $d = 1$, respectively. The proposed model replicates Matthiessen's rule for $d = 0$ and $f \ll 1$ and also accounts for defect-induced modifications for larger values of f while considering the dimensionality of the defect structure in the material. The time constant τ corresponds to a characteristic ion fluence $\Phi_{ch} = J_B\tau/q$ at which the resistance experiences a notable increase. Here, q is the elementary charge unit of the projectile ion.

The model function in Equation (1) was fitted to the resistance of both of the irradiated YBCO thin film bridges, and very good agreement was obtained (see Figure 4). For film bridge 2, ion-irradiated at $T = 100$ K, the strongly superlinear variation of resistance with time of irradiation is well described by the model function (light-blue solid line in Figure 4). The fit parameters are given in Table 1; the coefficient of determination was $\text{CoD} = 99.994\%$, and the chi-square value was $\chi^2 = 0.02636$. The spatial distribution of irradiation-induced defects was assumed to be independent of the sample temperature. Therefore, the same value of parameter d was used for the other bridge. The resistance increase in film bridge 1, ion-irradiated at $T = 295$ K, is also well described by this model (light-gray solid line in Figure 4; $\text{CoD} = 99.894\%$, $\chi^2 = 0.00081$).

Table 1. Time constant τ , resistivity increase r , dimensionality parameter d , and characteristic ion fluence Φ_{ch} of YBCO thin films irradiated with 75 keV He^+ ions at different sample temperatures. Parameters were determined from fits of the model function Equation (1) to the normalized resistance $R(t)/R_0$ data.

Parameter	Bridge 2 ($T = 100$ K)	Bridge 1 ($T = 295$ K)
τ (min)	5.83 ± 0.02	21.60 ± 0.08
r	422 ± 10	7.06 ± 0.06
d	0.294 ± 0.003	0.294
Φ_{ch} (10^{15} cm^{-2})	0.293 ± 0.001	0.825 ± 0.003

The shorter time constant and lower characteristic ion fluence, as well as the higher resistivity increase observed for bridge 2, demonstrate a more efficient modification of YBCO films when He^+ irradiation is conducted at low temperature as opposed to the irradiation at room temperature of bridge 1. This is attributed to a temperature-dependent "annealing process" for some of the irradiation defects. The relaxation of resistance sub-

sequent to irradiation at $T = 295$ K (Figure 1) and during warm-up after irradiation at $T = 100$ K (Figure 3) supports this conclusion. Despite its relaxation, the resistance of irradiated YBCO films remains well above the intrinsic resistance prior to irradiation, persisting at elevated levels even after months of sample storage at room temperature. This shows that the irradiation process generates a significant density of stable defects. A more sophisticated model that includes the formation of multiple defects in the same unit cell and the temperature-dependent relaxation of defects could result in even more precise fits to the $R(t)/R_0$ data obtained through measurement.

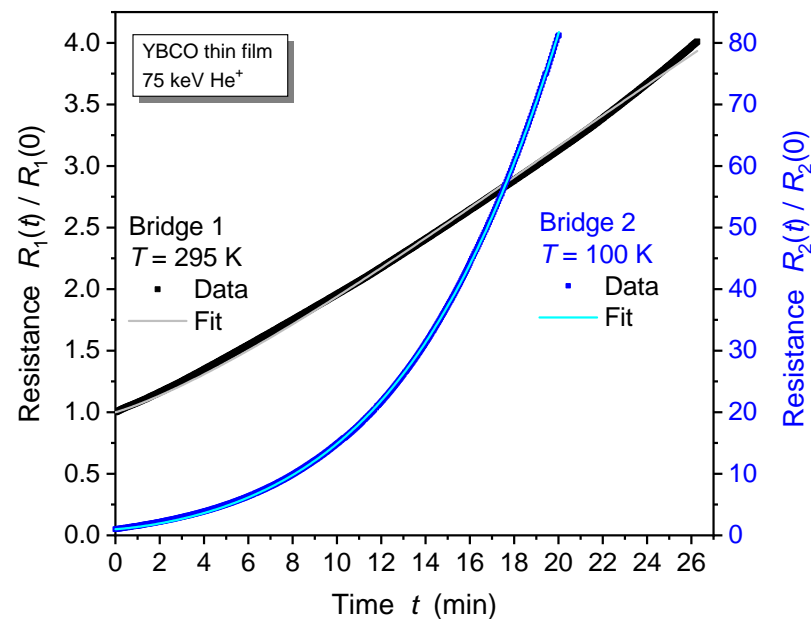


Figure 4. Normalized resistance of YBCO thin film during 75 keV He^+ irradiation of bridge 1 at room temperature (black symbols) and bridge 2 at $T = 100$ K (blue symbols). Solid lines are fits to the data. The dimensionality parameter extracted from the fit at $T = 100$ K was used as a fixed parameter for the fit of the data at 295 K as well.

2.2. Defect Relaxation during Thermal Annealing

The results of the previous measurements unequivocally demonstrate a thermally activated or assisted defect relaxation process. Therefore, we now aim to determine the activation energy for this phenomenon. While there is extensive literature on the diffusion and the activation energy of oxygen in- and out-diffusion in YBCO [32] as well as damage healing after heavy ion bombardment [33], little is known about defect healing of point defects resulting from light-ion irradiation [22,23].

Two 190 nm thick YBCO films were deposited on MgO and irradiated at room temperature with 75 keV He^+ ions with fluences of $0.7 \cdot 10^{15}$ ions/cm² (sample A) and $1.4 \cdot 10^{15}$ ions/cm² (sample B). The temperature-dependent resistivity of the samples measured before and after ion irradiation reveals a high T_{c0} of 90 K for the pristine sample and suppression of superconductivity in irradiated samples (Figure 5). After irradiation, the resistivity of sample B was much higher than in sample A due to the higher irradiation fluence.

For the annealing experiments, the ion-irradiated samples were placed in a quartz tube and heated in an inert Ar atmosphere while the change in resistance was recorded. Annealing temperatures were selected to be below 150 °C because previous test experiments suggested that at higher temperatures, the measurements could be affected by oxygen loss. Reduction of the oxygen content would lead to an increase in resistivity, possibly obscuring the effects of thermally activated diffusion of the displaced oxygen atoms [34]. After warming up the sample to the target temperature and waiting for stable conditions, the resistivity decay was recorded. A representative behavior of defect annealing is depicted

in the inset of Figure 6 for sample A at temperature $T = 102\text{ }^{\circ}\text{C}$. The broken gray line confirms a perfect exponential decay of the resistivity with time. Subsequently, sample A was heated to $T = 126\text{ }^{\circ}\text{C}$ and the measurement was repeated. A similar protocol was used for sample B, encompassing more temperatures, namely, $64\text{ }^{\circ}\text{C}$, $81\text{ }^{\circ}\text{C}$, $101\text{ }^{\circ}\text{C}$, $119\text{ }^{\circ}\text{C}$, and $142\text{ }^{\circ}\text{C}$.

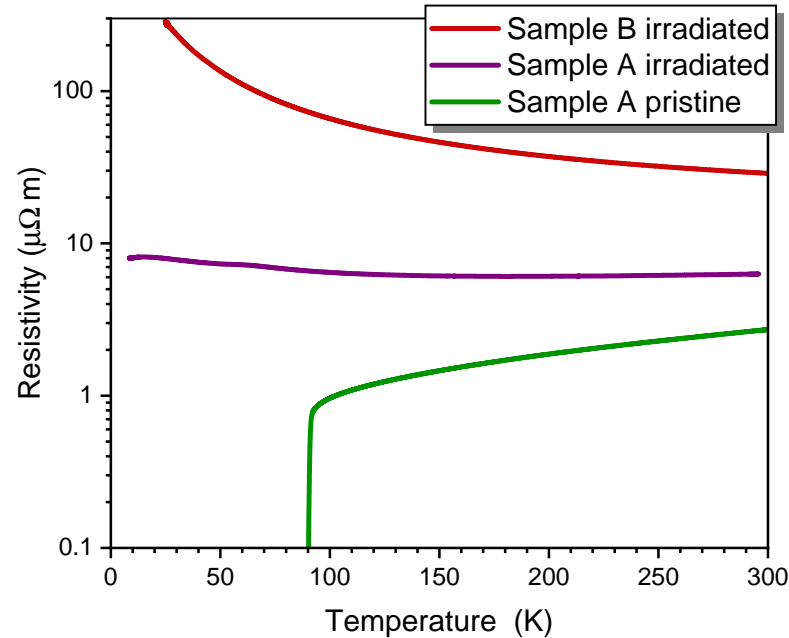


Figure 5. Temperature dependence of the resistivities of thin YBCO films: sample A before (green) and after irradiation with 75 keV He^+ at a fluence of 0.7×10^{15} ions/ cm^2 (lilac) and sample B after irradiation with a fluence of 1.4×10^{15} ions/ cm^2 (red).

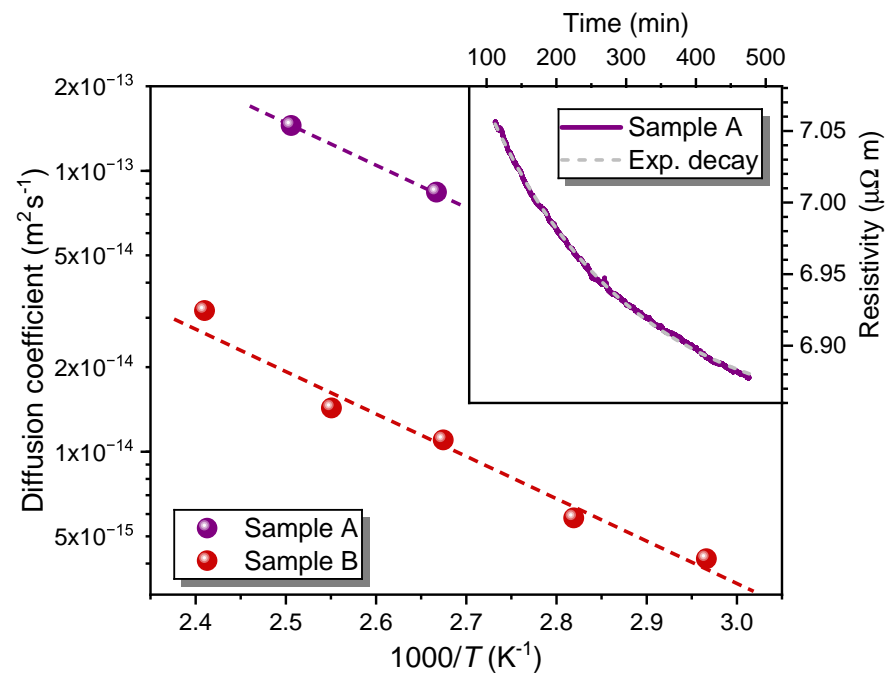


Figure 6. Diffusion—coefficient D of oxygen in samples A and B after ion irradiation, determined from the exponential decay of the resistivity. Samples were kept at constant temperatures in the argon atmosphere. The broken lines are fits to determine the activation energy for the rearrangement of oxygen atoms. The inset shows a representative example of the resistivity decrease in sample A at $102\text{ }^{\circ}\text{C}$.

For further analysis, we utilize the isothermal electric resistance relaxation technique, a common method for investigating oxygen diffusion in high-temperature superconductors [35]. It allows us to calculate the diffusion coefficients D at a given temperature T by measuring the change in resistivity ρ over time t and subsequently determine the required activation energy ΔE in YBCO thin films that have been irradiated with He^+ ions.

The method is based on the relationship between oxygen concentration within the CuO_2 planes and the CuO chains of YBCO with resistivity. Since measuring the oxygen concentration within these CuO chains is challenging, the changes in resistivity are assumed to be linearly correlated with the oxygen defects in the sample [36].

The increase in resistivity during light-ion irradiation is mostly caused by the displacement of weakly bound oxygen atoms from the copper-oxide chains. These oxygen atoms are only bound by approximately 1 eV [37], which is much lower compared to oxygen in CuO_2 planes (8 eV) [17] or any of the other components: yttrium (25 eV), barium (30 eV), and copper (15 eV) [38]. As a result, most irradiation-induced displacements are oxygen atoms from the chains [21] that are displaced by a small distance from their original position while not decreasing the oxygen content in the sample [23]. It is commonly assumed that the displaced oxygen species are often lodged along the a axis of the basal plane of the YBCO unit cell [39], where minimal energy is needed to shift them back into place again [23].

Annealing can be used to let the displaced oxygen diffuse back into place, thereby lowering the resistivity. It is important to note that this diffusion is a thermally activated process, and the changes in resistivity over time at a fixed annealing temperature need to be recorded. Since oxygen diffusion perpendicular to the CuO_2 layers in YBCO is negligible, predominant diffusion within the ab plane can be assumed [32].

Fick's second law can be used to describe this time-dependent diffusion process, which states

$$\frac{\partial c}{\partial t} = D \frac{\partial^2 c}{\partial x^2}. \quad (2)$$

In this scenario, we examine those oxygen atoms in YBCO which form the chains along the b axis. We consider their concentration c as a function of time t and position x . The diffusion coefficient D is defined by an Arrhenius equation that depends on the temperature T and the activation energy ΔE :

$$D(T) = D_0 \cdot \exp\left(-\frac{\Delta E}{k_B T}\right), \quad (3)$$

where D_0 is a material constant and k_B is the Boltzmann constant.

When solving Equation (2), we assume as the initial condition a homogeneous distribution of oxygen in the CuO chains of the sample and limit the process to the sample volume. This allows us to find a solution for the concentration. Subsequently, we can determine the relative changes in concentration [32].

$$\frac{c(t) - c_e}{c_0 - c_e} = \frac{8}{\pi^2} \cdot \exp\left(-\frac{t}{\tau}\right) \quad (4)$$

with

$$\tau = \frac{b^2}{\pi^2 D},$$

where c_e represents the saturation concentration, indicating the concentration of all the oxygen atoms positioned correctly in the CuO chains; c_0 is the starting concentration, and $c(t)$ is the concentration over time. The relaxation time τ depends on the sample width b and diffusion coefficient D .

Because measuring the concentration of oxygen in CuO-chain positions is hardly possible, we used the linear relationship between the concentration of displaced oxygen

atoms and resistivity from measurements at various ion fluences [23]. For temperatures low enough so only small changes in oxygen occur, Equation (4) can be converted to

$$\ln \left[\frac{\rho(t) - \rho_e}{\rho_0 - \rho_e} \frac{\pi^2}{8} \right] = -\frac{t}{\tau}, \quad (5)$$

where $\rho(t)$ is the time-dependent resistivity, ρ_0 is the initial resistivity of the irradiated sample before annealing, and ρ_e is the saturation resistivity for $t \rightarrow \infty$. For more details on the derivation of Equation (5), see [32].

In order to evaluate the oxygen diffusion coefficient $D(T)$ in the irradiated samples, we measured $\rho(t)$ during the annealing at temperature T and utilized Equation (5). Since ρ_e is not accessible experimentally, the measurements were performed over timescales significantly larger than τ and ρ_e determined from a fit of the exponential decay of $\rho(t)$ as exemplified in the inset of Figure 6. The values of D at several different temperatures are displayed as an Arrhenius plot in Figure 6. The slope of the fits (broken lines) allows us to determine the activation energy ΔE using Equation (3). Note, however, that the absolute values of D are subject to assumptions in the model that enter the prefactor D_0 , which has no influence on the determination of ΔE .

The results are $\Delta E_B = (0.31 \pm 0.03)$ eV for sample B and $\Delta E_A = 0.29$ eV for sample A. It is important to note that the value for sample A is based on only two measurements. Nonetheless, it still indicates that the activation energy is similar for different irradiation fluences. Other oxygen-diffusion experiments reported somewhat higher values for the activation energy, e.g., 1.23 eV [40], 0.8 eV [32], and 0.97 eV [41]. However, these experiments were conceptually different, as they measured the in- and out-diffusion of oxygen during annealing experiments in an oxygen atmosphere. In this scenario, diffusion is influenced by surface barriers [42], while in our experiments, the average oxygen content in the sample remains constant. A better-related study of defect recovery after irradiation with 500 keV He^+ ions corroborates our findings and found a value of $\Delta E = (0.36 \pm 0.05)$ eV [25].

2.3. Long-Term Stability of Nanopatterned YBCO Films

Nanopatterning of YBCO thin films by focused-ion-beam irradiation has proven to be a versatile method for fabricating ultradense vortex pinning landscapes and Josephson junctions. However, one might have concerns about their long-term stability due to oxygen migration that could blur the oxygen-defect profile [43]. Building on our previously presented experiments, we investigate the temporal evolution of the critical temperature, the resistivity, and the critical current of an 80 nm thick YBCO film on MgO substrate that was irradiated with a 30 keV He^+ focused ion beam in the HIM at room temperature. The columnar defects (CDs) were arranged in a square lattice with 200 nm spacings. More details on sample fabrication and properties are reported elsewhere [13].

The temporal evolution of the resistivity vs. temperature characteristics and the change in T_{c0} are illustrated in Figure 7 over a span of almost six years. The sample was kept in a desiccator at room temperature in the ambient atmosphere between measurements. It is important to emphasize that in our analysis we are only considering the days when the sample was stored at room temperature, as aging effects are minimal when the sample is kept in the cryostat at low temperature. After irradiation, the critical temperature decreased by approximately 3.5 K due to the inevitable straggle of some ions off their path, causing a minor amount of irradiation defects between the CDs. Over the storage period, T_{c0} initially increased and reached its maximum after approximately 3.4 years. For even longer storage periods, a marginal decrease in T_{c0} was found, accompanied by a small increase in the normal-state resistivity.

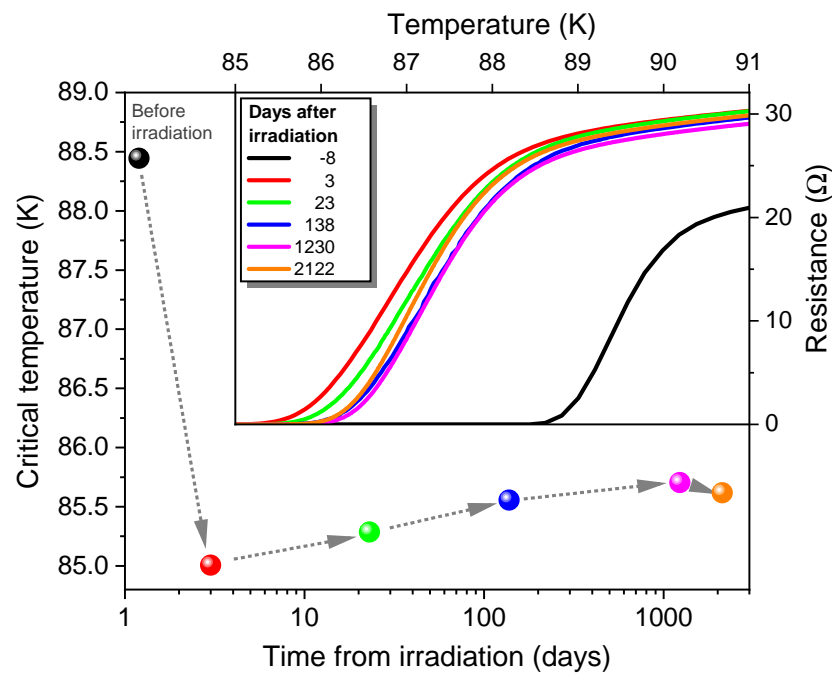


Figure 7. Zero-resistance critical temperature T_{c0} over room-temperature storage time in an 80 nm YBCO film before and after He-FIB irradiation imprinting a square pinning array of 200 nm spacings. The black bullet represents T_{c0} eight days before the irradiation. The arrows indicate the sequence of $\rho(T)$ measurements from which T_{c0} was determined, using a 10 m Ω criterion. Inset: Evolution of the resistance vs. temperature characteristics of the sample with room-temperature annealing time. The black line represents the $\rho(T)$ measurement of the sample before irradiation.

The long-term stability of unirradiated thin YBCO films has long been a topic of controversial discussion, especially with regard to effects of exposure to humidity and carbon dioxide in air [44]. Exposure to air causes YBCO to form hydroxide and carbonate layers on its surface [45]. Additionally, the commonly used photolithographic patterning exposes the *ab* planes of YBCO to the environment, which are more prone to environmental degradation [45].

However, for irradiated samples, a competition between defect healing after irradiation, which increases T_{c0} , and the above-mentioned deterioration of the sample through decomposition, which decreases T_{c0} , can be anticipated. In fact, we observe an increase in T_{c0} and a reduction in resistivity during storage in a desiccator up to a time span of approximately 3.4 years, which we attribute to a partial rearrangement of displaced oxygen atoms. The minor reversal of this trend at still longer times is probably connected with a saturation of the healing process and a small deterioration of the sample properties during dry-air exposure. Nevertheless, our data indicate a robust long-term stability of the nanopatterned YBCO films if kept in dry air.

Vortex commensurability effects occur when a magnetic field applied parallel to the CDs creates a vortex density that matches the sample's CD arrangement. Maxima of the critical current appear at so-called matching fields

$$B_k = k\Phi_0/A, \quad (6)$$

where k is the number of pinning sites (or vortices) in the unit cell of area A of the two-dimensional CD lattice, and $\Phi_0 = h/(2e)$ is the magnetic flux quantum. The square array of CDs in our nanopatterned sample features a unit cell of $A = (200 \text{ nm})^2$, leading to a first matching field $B_1 = 51.7 \text{ mT}$ [13]. A sketch of the pinning lattice (green circles) and the positions of the trapped vortices (blue dots) at the first matching field is shown in the inset of Figure 8.

The sample was kept at room temperature for three days after irradiation in the HIM before we conducted an initial measurement of the critical current in the superconducting state at $T = 84.1$ K (red circles in Figure 8). Another measurement was performed 2122 days later under the same conditions (blue circles). The matching field is identical, indicating that the pinning landscape is still efficient and leads to the same vortex arrangement. However, the overall critical current has increased over the entire magnetic field range. In particular, its value at B_1 became 5.8 times larger. At first glance, this could be due to the decrease in the relative temperature T/T_{c0} as a result of the higher T_{c0} , as shown in Figure 7. Typically, the critical current significantly increases at temperatures further below T_{c0} . However, upon closer inspection of an additional measurement taken at the same $T/T_{c0} = 0.989$ as the initial measurement, it is revealed that the critical current is still enhanced by a factor of 1.9 after long-term storage.

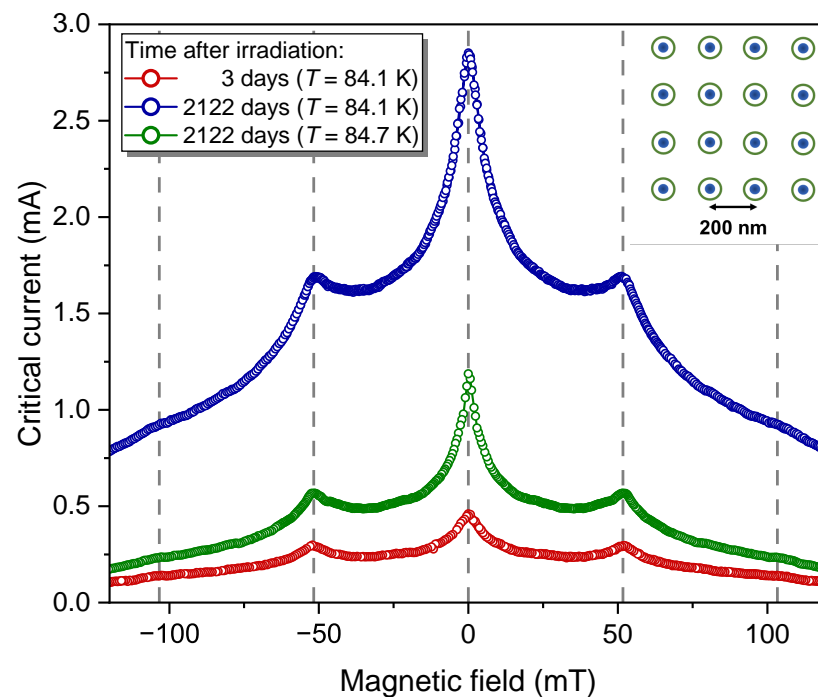


Figure 8. Temporal evolution of the critical current in an 80 nm YBCO film structured by He-FIB into a square array of defect columns with 200 nm spacings. The initial critical current measurement after irradiation is denoted by red circles, while the subsequent measurement following 2122 days (almost six years) of storage in dry air at room temperature is represented by blue circles. The green symbols show the corresponding measurement at 84.7 K, taken at the same reduced temperature $T/T_{c0} = 0.989$ as the measurement before long-term storage. Gray broken lines represent the magnetic fields according to Equation (6) with values $k = \{-2, -1, 0, 1, 2\}$. Inset: Layout of the pinning lattice, where green circles represent the columnar defects and blue dots denote the positions of the trapped vortices for $k = \pm 1$.

The long-term resilience of the matching peaks can be understood as follows: The spreading of the penetrating He^+ ions causes a “damage gradient” perpendicular to its initial trajectory. The density of defects in the center of the defect column is high enough to withstand room-temperature annealing. However, the defect density rapidly decreases with the distance from the center [14]. These inter-CD regions are primarily susceptible to healing effects which potentially can “sharpen” the defect profile around the CDs due to Frenkel defect recombination [46] and ultimately lead to the observed increase in T_{c0} , the reduction of the resistivity, and the increase in the critical current at the matching field.

Indeed, studies on He-FIB-created Josephson junctions (JJs) found that aging at room temperature in a nitrogen environment resulted in a significant enhancement of the critical

current, with timescales that are highly dependent on the irradiation dose. Annealing at 90 °C under low and high oxygen pressures confirmed that the modifications in the JJs' characteristics stem from repositioning oxygen atoms to their original sites rather than restoring the oxygen content in the films [20]. This discovery rules out the possibility of oxygen depletion during He⁺-ion irradiation, aligning with electrical transport measurements [14]. Other works reported good temporal stability of JJs prepared by masked Ne⁺-ion irradiation over eight years [47] and investigated the voltage modulation of current-biased JJ arrays as a function of the applied magnetic field. The increase in the voltage modulation after post-annealing at 100 °C in oxygen resulted from a narrowing of the barrier by diffusion and recombination of the low-energy oxygen defects [21].

The findings of these various experiments indicate that controlled annealing at temperatures moderately above room temperature could be a tool to enhance the properties of nanostructures created by He-FIB in a reasonably short timescale while also anticipating healing effects and thus increasing their long-term stability.

3. Methods and Materials

3.1. YBCO Thin Film Production

All YBCO thin films in this work were produced by pulsed laser deposition (PLD) [48]. Films were grown on single-crystal MgO (100) substrates. A stoichiometric YBCO ceramic fabricated via the solid-state reaction method was used as the target. Ablation was carried out with a KrF-excimer laser ($\lambda = 248$ nm) at a pulse repetition rate of 10 Hz with a pulse duration of 25 ns and a fluence of 3.25 J/cm². The deposition took place at a substrate temperature of 750 °C in a 0.7 mbar oxygen background. Annealing at 450 °C in 800 mbar oxygen background was carried out for 30 min. Finally, the films were patterned by wet-chemical etching via a photolithographic mask to define geometries suitable for four-point resistance measurements.

3.2. Irradiation of Thin Films

The irradiation of YBCO using a collimated He⁺-ion beam was performed on an ion implanter (High Voltage Engineering Europa B.V., Amersfoort, the Netherlands), using a metal mask to shield the electrical contacts of the sample. The setup allowed for cooling of the sample during irradiation by a flow of liquid nitrogen while also measuring the resistance. He⁺ ions with 75 keV energy were used, with 99% of them exiting the YBCO film without being implanted at this energy level. To prevent channeling of He⁺ ions along the *c* axis of the sample, the ion incidence angle was set to 5° off the surface normal. The ion fluence was monitored by Faraday cups, and the irradiation was halted once the desired, preset fluence was achieved. The ion beam current density was kept below 0.25 $\mu\text{A}/\text{cm}^2$ to avoid inducing thermal effects during irradiation.

The irradiated nanostructures were prepared using a HIM (ORION NanoFab, Carl Zeiss Microscopy, Oberkochen, Germany). An array of irradiated spots with a diameter of ≈ 50 nm was created with a slightly defocused 30 keV He⁺-ion beam at a beam current of 3.0 pA. A total of 50,000 ions per defect column were used to form the pinning array. More detailed information on creating the array of columnar defects via HIM and comprehensive measurements on the nanoirradiated samples can be found in [13].

3.3. Annealing of Thin Films

To anneal the samples above room temperature, they were placed in a quartz-glass tube inside a tube furnace (Heraeus RO 4/25, Hanau, Germany) with a temperature controller. A minimal overpressure of flowing Ar gas, controlled by a gas-washing bottle at the back end of the quartz tube, was maintained. We made sure that the gas flow did not compromise the temperature stability, and the sample temperature was continuously monitored by a platinum (Pt-100) sensor.

3.4. Electrical Characterization of Thin Films

The in situ resistivity measurements of the films during and after irradiation were performed with a constant current supply (Keithley Instruments 224, Solon, OH, USA), with a measurement current of 1 μA , and a nanovoltmeter (Keithley Instruments SDV 182, Solon, OH, USA).

The setup for the determination of the oxygen diffusion coefficient and the activation energy consisted of a different current supply (Keithley Instruments 6221, Solon, OH, USA) and nanovoltmeter (Keithley Instruments 2182A, Solon, OH, USA). Here, a measurement current of 10 μA was chosen.

Electrical transport measurements in magnetic fields were conducted on the HIM-structured samples using a closed-cycle cryocooler positioned between the poles of an electromagnet. The setup allows for precise temperature adjustments with a stability of approximately 1 mK. This was achieved by employing a ceramic temperature sensor (Cernox-1080, Lake Shore Cryotronics, Woburn, MA, USA) in conjunction with a temperature controller (LakeShore Cryotronics 336, Woburn, MA, USA). Critical currents were determined using a 100 nV criterium, corresponding to an electrical field of 10 $\mu\text{V}/\text{cm}$.

4. Conclusions

In summary, we examined the long-term stability and the annealing of defects created by He^+ -ion irradiation in thin YBCO films in in situ and ex situ experiments. The increase in resistivity depends strongly on the temperature at which the sample is kept during irradiation and can be described by a phenomenological model; while a decrease in resistivity occurs within minutes after stopping the irradiation at room temperature, no such relaxation is seen at 100 K. The counteracting creation and healing of oxygen displacements is, therefore, an important consideration for the chosen irradiation temperature.

Monitoring the resistivity evolution at several elevated temperatures, where oxygen out-diffusion can still be ruled out, allowed us to determine the diffusion coefficients for rearranging oxygen atoms into their original sites. The activation energy $\Delta E = (0.31 \pm 0.03)$ eV of this process is lower than the one for oxygen diffusion out of the YBCO film, making it possible to improve sample properties by annealing at selected temperatures without deoxygenating them.

Since focused He^+ -ion-beam irradiation is an extremely versatile tool to modulate the superconducting properties, we investigated the aging of vortex-pinning arrays over long timescales. During the initial healing period, T_c slightly increased during 3.4 years and only marginally decreased thereafter. The general reduction of resistivity did not compromise the vortex-matching signatures. On the contrary, we observed a dramatic increase in the critical current in the whole range of magnetic fields under investigation that is most notable at zero field and at the matching peaks. Our analysis suggests that long-term room-temperature annealing maintains the robust pinning potential at the cores of the columnar defect channels while reducing the defect density surrounding them. These results indicate the long-term stability of He^+ -ion-irradiated YBCO films at room temperature following an initial enhancement during a healing phase, and they underscore the robustness of structures fabricated using a focused He^+ -ion beam. This has significant implications for potential applications in fluxonics.

Author Contributions: Conceptualization, J.D.P., D.K. and W.L.; methodology, B.A., B.M., J.D.P., D.K. and W.L.; validation, S.K., J.D.P., B.A. and W.L.; formal analysis, S.K., B.A., P.R., M.-A.B., J.D.P. and W.L.; investigation, B.A., B.M., P.R., M.K. and M.-A.B.; resources, J.D.P., R.K., E.G., D.K. and W.L.; data curation, J.D.P. and W.L.; writing—original draft preparation, S.K.; writing—review and editing, J.D.P. and W.L.; visualization, S.K. and B.A.; supervision, J.D.P., R.K., D.K. and W.L.; project administration, J.D.P., E.G., D.K. and W.L.; funding acquisition, J.D.P., D.K. and W.L. All authors have read and agreed to the published version of the manuscript.

Funding: The research was funded in whole, or in part, by the Austrian Science Fund (FWF) grant I4865-N and the German Research Foundation (DFG), grant KO 1303/16-1. For the purpose of open access, the authors have applied a CC-BY public copyright license to any Author Accepted Manuscript version arising from this submission. The research is based upon work from COST Actions CA21144 (SuperQuMap), CA19140 (FIT4NANO), and CA19108 (Hi-SCALE) supported by COST (European Cooperation in Science and Technology).

Institutional Review Board Statement: Not applicable.

Informed Consent Statement: Not applicable.

Data Availability Statement: Data are available on reasonable request from the corresponding author.

Acknowledgments: Open Access Funding by the University of Vienna.

Conflicts of Interest: Author Marius-Aurel Bodea is employed by the Infineon Technologies Austria AG. All authors declare that the research was conducted at universities in the absence of any commercial or financial relationships that could be construed as a potential conflict of interest.

References

1. Kahlmann, F.; Engelhardt, A.; Schubert, J.; Zander, W.; Buchal, C.; Hollkott, J. Superconductor-normal-superconductor Josephson junctions fabricated by oxygen implantation into $\text{YBa}_2\text{Cu}_3\text{O}_{7-\delta}$. *Appl. Phys. Lett.* **1998**, *73*, 2354. [[CrossRef](#)]
2. Katz, A.S.; Sun, A.G.; Woods, S.I.; Dynes, R.C. Planar thin film $\text{YBa}_2\text{Cu}_3\text{O}_{7-\delta}$ Josephson junctions via nanolithography and ion damage. *Appl. Phys. Lett.* **1998**, *72*, 2032. [[CrossRef](#)]
3. Bergeal, N.; Grison, X.; Lesueur, J.; Faini, G.; Aprili, M.; Contour, J.P. High-quality planar high- T_c Josephson junctions. *Appl. Phys. Lett.* **2005**, *87*, 102502. [[CrossRef](#)]
4. Cybart, S.A.; Cho, E.Y.; Wong, T.J.; Wehlin, B.H.; Ma, M.K.; Huynh, C.; Dynes, R.C. Nano Josephson superconducting tunnel junctions in $\text{YBa}_2\text{Cu}_3\text{O}_{7-\delta}$ directly patterned with a focused helium ion beam. *Nat. Nanotechnol.* **2015**, *10*, 598. [[CrossRef](#)]
5. Müller, B.; Karrer, M.; Limberger, F.; Becker, M.; Schröppel, B.; Burkhardt, C.J.; Kleiner, R.; Goldobin, E.; Koelle, D. Josephson Junctions and SQUIDS Created by Focused Helium-Ion-Beam Irradiation of $\text{YBa}_2\text{Cu}_3\text{O}_7$. *Phys. Rev. Appl.* **2019**, *11*, 044082. [[CrossRef](#)]
6. Bergeal, N.; Lesueur, J.; Faini, G.; Aprili, M.; Contour, J.P. High T_c superconducting quantum interference devices made by ion irradiation. *Appl. Phys. Lett.* **2006**, *89*, 112515. [[CrossRef](#)]
7. Li, H.; Cai, H.; Cho, E.Y.; McCoy, S.J.; Wang, Y.T.; LeFebvre, J.C.; Zhou, Y.W.; Cybart, S.A. High-transition-temperature nanoscale superconducting quantum interference devices directly written with a focused helium ion beam. *Appl. Phys. Lett.* **2020**, *116*, 070601. [[CrossRef](#)]
8. Ouanani, S.; Kermorvant, J.; Ulysse, C.; Malnou, M.; Lemaître, Y.; Marcihac, B.; Feuillet-Palma, C.; Bergeal, N.; Crété, D.; Lesueur, J. High- T_c superconducting quantum interference filters (SQIFs) made by ion irradiation. *Supercond. Sci. Technol.* **2016**, *29*, 094002. [[CrossRef](#)]
9. Swiecicki, I.; Ulysse, C.; Wolf, T.; Bernard, R.; Bergeal, N.; Briatico, J.; Faini, G.; Lesueur, J.; Villegas, J.E. Strong field-matching effects in superconducting $\text{YBa}_2\text{Cu}_3\text{O}_{7-\delta}$ films with vortex energy landscapes engineered via masked ion irradiation. *Phys. Rev. B* **2012**, *85*, 224502. [[CrossRef](#)]
10. Trastoy, J.; Malnou, M.; Ulysse, C.; Bernard, R.; Bergeal, N.; Faini, G.; Lesueur, J.; Briatico, J.; Villegas, J.E. Freezing and thawing of artificial ice by thermal switching of geometric frustration in magnetic flux lattices. *Nat. Nanotechnol.* **2014**, *9*, 710. [[CrossRef](#)]
11. Haag, L.T.; Zechner, G.; Lang, W.; Dosmailov, M.; Bodea, M.A.; Pedarnig, J.D. Strong vortex matching effects in YBCO films with periodic modulations of the superconducting order parameter fabricated by masked ion irradiation. *Physica C* **2014**, *503*, 75. [[CrossRef](#)]
12. Zechner, G.; Lang, W.; Dosmailov, M.; Bodea, M.A.; Pedarnig, J.D. Transverse vortex commensurability effect and sign change of the Hall voltage in superconducting $\text{YBa}_2\text{Cu}_3\text{O}_{7-\delta}$ thin films with a nanoscale periodic pinning landscape. *Phys. Rev. B* **2018**, *98*, 104508. [[CrossRef](#)]
13. Aichner, B.; Müller, B.; Karrer, M.; Misko, V.R.; Limberger, F.; Mletschnig, K.L.; Dosmailov, M.; Pedarnig, J.D.; Nori, F.; Kleiner, R.; et al. Ultradense Tailored Vortex Pinning Arrays in Superconducting $\text{YBa}_2\text{Cu}_3\text{O}_{7-\delta}$ Thin Films Created by Focused He Ion Beam Irradiation for Fluxonics Applications. *ACS Appl. Nano Mater.* **2019**, *2*, 5108. [[CrossRef](#)]
14. Karrer, M.; Aichner, B.; Wurster, K.; Magén, C.; Schmid, C.; Hutt, R.; Budinská, B.; Dobrovolskiy, O.V.; Kleiner, R.; Lang, W.; et al. Vortex matching at 6 T in $\text{YBa}_2\text{Cu}_3\text{O}_{7-\delta}$ thin films by imprinting a 20-nm periodic pinning array with a focused helium-ion beam. *Phys. Rev. Appl.* **2024**, *22*, 014043. [[CrossRef](#)]
15. Lesueur, J.; Dumoulin, L.; Quillet, S.; Radcliffe, J. Ion-beam induced metal insulator transition in YBCO films. *J. Alloy. Compd.* **1993**, *195*, 527. [[CrossRef](#)]
16. Civale, L. Vortex pinning and creep in high-temperature superconductors with columnar defects. *Supercond. Sci. Technol.* **1997**, *10*, A11. [[CrossRef](#)]

17. Tolpygo, S.K.; Lin, J.Y.; Gurvitch, M.; Hou, S.Y.; Phillips, J.M. Effect of oxygen defects on transport properties and T_c of $\text{YBa}_2\text{Cu}_3\text{O}_{6+x}$: Displacement energy for plane and chain oxygen and implications for irradiation-induced resistivity and T_c suppression. *Phys. Rev. B* **1996**, *53*, 12462. [[CrossRef](#)]
18. Meyer, O.; Kroener, T.; Rimmel, J.; Geerk, J.; Linker, G.; Strehlau, B.; Wolf, T. Transport and structure of ion irradiated HTSC thin films. *Nucl. Instr. Meth. Phys. Res. B* **1992**, *65*, 539. [[CrossRef](#)]
19. Lang, W.; Richter, H.; Marksteiner, M.; Siraj, K.; Bodea, M.A.; Pedarnig, J.D.; Grigoropoulos, C.; Bäuerle, D.; Hasenfuss, C.; Palmeshofer, L.; et al. Masked ion beam irradiation of high-temperature superconductors: Patterning of nano-size regions with high point-defect density. *Int. J. Nanotechnol.* **2009**, *6*, 704. [[CrossRef](#)]
20. Karrer, M.; Wurster, K.; Linek, J.; Meichsner, M.; Kleiner, R.; Goldobin, E.; Koelle, D. Temporal evolution of electric transport properties of $\text{YBa}_2\text{Cu}_3\text{O}_{7-\delta}$ Josephson junctions produced by focused-helium-ion-beam irradiation. *Phys. Rev. Appl.* **2024**, *21*, 014065. [[CrossRef](#)]
21. Cho, E.Y.; Kouperine, K.; Zhuo, Y.; Dynes, R.C.; Cybart, S.A. The effects of annealing a 2-dimensional array of ion-irradiated Josephson junctions. *Supercond. Sci. Technol.* **2016**, *29*, 094004. [[CrossRef](#)]
22. Markowitsch, W.; Steiger, B.; Lang, W.; Bodea, M.A.; Pedarnig, J.D. Optically induced changes and long-term relaxations of resistivity and critical temperature in He^+ irradiated $\text{YBa}_2\text{Cu}_3\text{O}_x$. *Thin Solid Film.* **2010**, *518*, 7070. [[CrossRef](#)]
23. Arias, D.; Sefrioui, Z.; Loos, G.D.; Agullo-Rueda, F.; Garcia-Barriocanal, J.; Leon, C.; Santamaria, J. Pair breaking by chain oxygen disorder in light-ion irradiated $\text{YBa}_2\text{Cu}_3\text{O}_x$ thin films. *Phys. Rev. B* **2003**, *68*, 94515. [[CrossRef](#)]
24. Wang, X.Z.; Hellebrand, B.; Bäuerle, D.; Strecker, M.; Wortmann, G.; Lang, W. Oxygen ordering and superconductivity in $\text{GdBaSrCu}_3\text{O}_{7-x}$. *Physica C* **1995**, *242*, 55. [[CrossRef](#)]
25. Barbour, J.C.; Venturini, E.L.; Ginley, D.S.; Kwak, J.F. Irradiation Effects in High-Temperature Superconductors. *Nucl. Instr. Meth. Phys. Res. Sect. B* **1992**, *65*, 531. [[CrossRef](#)]
26. Liu, J.; Zhang, Z.; Wu, J.; Ma, K.; Zhao, Y.; Yu, N.; Hsieh, P.; Chu, W.K. Fluorine and hydrogen ion irradiation in YBaCuO superconductor. *Nucl. Instrum. Methods Phys. Res. Sect. B* **1991**, *62*, 74. [[CrossRef](#)]
27. Iliffe, W.; Peng, N.; Brittlens, G.; Bateman, R.; Webb, R.; Grovenor, C.; Speller, S. In-situ measurements of the effect of radiation damage on the superconducting properties of coated conductors. *Supercond. Sci. Technol.* **2021**, *34*, 09LT01. [[CrossRef](#)]
28. Jaouen, C.; Delafond, J.; Riviere, J.P. Crystalline to amorphous transformation in NiAl: Ion irradiation studies in relation to cascade parameters. *J. Phys. F Met. Phys.* **1987**, *17*, 335. [[CrossRef](#)]
29. Miranda, R.M.N.; Vasconcellos, M.A.Z.; Baibich, M.N.; Borges da Costa, J.A.T. Depth dependence of electrical resistivity transformations by ion beams. *Nucl. Instrum. Methods Phys. Res. Sect. B* **1997**, *127–128*, 132. [[CrossRef](#)]
30. Karpe, N. Using electrical resistivity to analyze the kinetics of irradiation induced amorphization of metals. *Nucl. Instrum. Methods Phys. Res. Sect. B* **1995**, *95*, 485. [[CrossRef](#)]
31. Christian, J. *The Theory of Transformations in Metals and Alloys*; Pergamon: Oxford, UK, 2002.
32. Erb, A.; Greb, B.; Müller-Vogt, G. In-situ resistivity measurements during the oxygenation of $\text{YBa}_2\text{Cu}_3\text{O}_{7-\delta}$ and $\text{Gd}_{0.8}\text{Y}_{0.2}\text{Ba}_2\text{Cu}_3\text{O}_{7-\delta}$ single crystals. *Physica C* **1996**, *259*, 83. [[CrossRef](#)]
33. Matsui, S.; Matsutera, H.; Yoshitake, T.; Fujita, J.; Ichihashi, T.; Mito, M. Ion and electron beam irradiation effects for high- T_c superconducting thin films. *Radiat. Eff. Defect. S.* **1992**, *124*, 81. [[CrossRef](#)]
34. Mesarwi, A.; Levenson, L.L.; Ignatiev, A. Oxygen desorption from $\text{YBa}_2\text{Cu}_3\text{O}_{7-x}$ and $\text{Bi}_2\text{CaSr}_2\text{Cu}_2\text{O}_{8+\delta}$ superconductors. *J. Appl. Phys.* **1991**, *70*, 1591. [[CrossRef](#)]
35. Zhang, H.; Ye, H.; Du, K.; Huang, X.Y.; Wang, Z.H. Electric resistance relaxation and oxygen diffusion in melt-texture grown YBCO bulk post-annealed at high temperature. *Supercond. Sci. Technol.* **2002**, *15*, 1268. [[CrossRef](#)]
36. Diosa, J.E.; Vargas, R.A.; Mellander, B.E. Oxygen diffusion in $\text{Y}_{1-x}\text{Pr}_x\text{Ba}_2\text{Cu}_3\text{O}_{7-\delta}$ observed by resistivity measurements. *J. Phys. Condens. Matter* **1997**, *9*, 4621. [[CrossRef](#)]
37. Cui, F.Z.; Xie, J.; Li, H.D. Preferential radiation damage of the oxygen sublattice in $\text{YBa}_2\text{Cu}_3\text{O}_7$: A molecular-dynamics simulation. *Phys. Rev. B* **1992**, *46*, 11182. [[CrossRef](#)] [[PubMed](#)]
38. Kirsanov, V.V.; Musin, N.N.; Shamarina, H.J. Displacement threshold energy in high-temperature superconductors. II. Thresholds for O, Ba and Y in $\text{YBa}_2\text{Cu}_3\text{O}_7$. *Phys. Lett. A* **1992**, *171*, 223. [[CrossRef](#)]
39. Valles, J.M.; White, A.E.; Short, K.T.; Dynes, R.C.; Garno, J.P.; Levi, A.F.J.; Anzlowar, M.; Baldwin, K. Ion-beam-induced metal-insulator transition in $\text{YBa}_2\text{Cu}_3\text{O}_{7-\delta}$: A mobility edge. *Phys. Rev. B* **1989**, *39*, 11599. [[CrossRef](#)] [[PubMed](#)]
40. Chen, Y.X.; Zhang, J.; Wu, Z. Oxygen diffusion in c-axis-oriented $\text{YBa}_2\text{Cu}_3\text{O}_x$ films. *Supercond. Sci. Technol.* **1992**, *5*, 463. [[CrossRef](#)]
41. Rothman, S.J.; Routbort, J.L.; Welp, U.; Baker, J.E. Anisotropy of oxygen tracer diffusion in single-crystal $\text{YBa}_2\text{Cu}_3\text{O}_{7-\delta}$. *Phys. Rev. B* **1991**, *44*, 2326. [[CrossRef](#)]
42. Tu, K.N.; Yeh, N.C.; Park, S.I.; Tsuei, C.C. Diffusion of oxygen in superconducting $\text{YBa}_2\text{Cu}_3\text{O}_{7-\delta}$ ceramic oxides. *Phys. Rev. B* **1989**, *39*, 304. [[CrossRef](#)] [[PubMed](#)]
43. Zaluzhnyy, I.A.; Goteti, U.; Stoychev, B.K.; Basak, R.; Lamb, E.S.; Kisiel, E.; Zhou, T.; Cai, Z.; Holt, M.V.; Beeman, J.W.; et al. Structural Changes in $\text{YBa}_2\text{Cu}_3\text{O}_7$ Thin Films Modified with He^+ -Focused Ion Beam for High-Temperature Superconductive Nanoelectronics. *ACS Appl. Nano Mater.* **2024**. [[CrossRef](#)]
44. Gherardi, L.; Metra, P.; Vellego, G.; Radaelli, P. Critical current decay with ageing for polycrystalline YBCO wires and rings. *Cryogenics* **1990**, *30*, 576. [[CrossRef](#)]

45. Behner, H.; Rührschopf, K.; Wedler, G.; Rauch, W. Surface reactions and long time stability of YBCO thin films. *Phys. C* **1993**, *208*, 419. [[CrossRef](#)]
46. Sirena, M.; Matzen, S.; Bergeal, N.; Lesueur, J.; Faini, G.; Bernard, R.; Briatico, J.; Crété, D.G. Annealing of ion irradiated high T_c Josephson junctions studied by numerical simulations. *J. Appl. Phys.* **2009**, *105*, 023910. [[CrossRef](#)]
47. Cybart, S.A.; Roediger, P.; Chen, K.; Parker, J.M.; Cho, E.Y.; Wong, T.J.; Dynes, R.C. Temporal Stability of Y–Ba–Cu–O Nano Josephson Junctions from Ion Irradiation. *IEEE Trans. Appl. Supercond.* **2013**, *23*, 1100103. [[CrossRef](#)]
48. Bäuerle, D. *Laser Processing and Chemistry*; Springer Science & Business Media: Berlin/Heidelberg, Germany, 2013.

Disclaimer/Publisher’s Note: The statements, opinions and data contained in all publications are solely those of the individual author(s) and contributor(s) and not of MDPI and/or the editor(s). MDPI and/or the editor(s) disclaim responsibility for any injury to people or property resulting from any ideas, methods, instructions or products referred to in the content.